Mon. Not. R. Astron. Soc. **297,** 265–277 (1998)

A multidimensional upwind scheme for magnetohydrodynamics

S. A. E. G. Falle,[1] S. S. Komissarov[1,2] and P. Joarder[1]
[1]*Department of Applied Mathematics, The University of Leeds, Leeds LS2 9JT*
[2]*Astrospace Centre, Lebedev Physical Institute, Leninsky Prospect 53, Moscow B-333, 177924 Russia*

Accepted 1998 January 23. Received 1997 December 1; in original form 1996 December 12

ABSTRACT

This paper describes a second-order upwind scheme for multidimensional magnetohydrodynamics, which uses a linear approximation for all Riemann problems except those involving strong rarefactions. This enables it to cope with initial data for which previously published schemes might fail. The condition $\nabla\cdot\boldsymbol{B} = 0$ is not enforced in multidimensions, but the numerical problems associated with this are dealt with by adding source terms to the equations, as suggested by Powell. We also show that there are advantages to adding second-order artificial dissipation at shocks.

Key words: MHD.

1 INTRODUCTION

There are numerous astrophysical objects that involve the motion of a conducting, compressible fluid containing a dynamically significant magnetic field (see e.g. Parker 1979). Examples include supernova remants, stellar wind bubbles, accretion discs, stars, planets, the solar wind and many others. In many cases the continuum approximation is valid, the fluid velocities are subrelativistic and the ohmic dissipation time is much longer than the dynamical time-scale, which means that one can use the equations of ideal magnetohydrodynamics (MHD). Although these equations also arise in a number of terrestrial applications, these do not usually involve shocks, whereas many of the astrophysical flows do. As in ordinary gas dynamics, the complexity of the equations is such that there are many important questions that require numerical calculations since they cannot be answered by analytic means. It is therefore important to develop numerical algorithms for the compressible MHD equations, which can cope with shocks and other discontinuites. Since experience has taught us that conservative upwind schemes are the most appropriate for ordinary gas dynamical flows with discontinuities (see e.g. Roe 1986), it is likely that such schemes will also be effective for MHD.

Although upwind schemes have been applied to relativistic hydrodynamics (e.g. Eulderink & Mellema 1994; Font et al. 1994; Falle & Komissarov 1996), it has not been quite so easy to extend them to MHD. The main reasons for this are that an exact solution to the Riemann problem is extremely complex (Gogosov 1961; Jeffreys & Taniuti 1964) and the fact that such schemes do not automatically ensure $\nabla\cdot\boldsymbol{B} = 0$.

The complexity of the Riemann problem need not worry us too much since there are a number of ways of constructing approximate solutions (e.g. Brio & Wu 1988; Zachary, Malagoli & Collela 1994; Ryu & Jones 1995) and codes based on these methods seem to work quite well. In any case, although an exact Riemann solver is expensive, this has little effect on the total computational cost if it is only invoked for the relatively small number of Riemann problems for which there is a large difference between the two states.

It is well known that although the exact equations preserve $\nabla\cdot\boldsymbol{B} = 0$, numerical schemes do not necessarily do so. Brackbill & Barnes (1980) have shown that this can cause conservative schemes to behave badly in regions where the forces are close to equilibrium. They suggest using the non-conservative form of the momentum equation, but this is clearly unsatisfactory for flows containing strong shocks. Zachary et al. (1994) therefore only use a non-conservative differencing for the troublesome terms. They also ensure that the field is divergence free by solving a Poisson equation for a pseudo-potential and then using this to correct the field. We prefer not to correct the field since not only is it is quite expensive to solve a Poisson equation, but their results suggest that it is not really necessary. It is however, essential to avoid the evil effects of a non-vanishing $\nabla\cdot\boldsymbol{B} = 0$. Some recent work by Powell (1994) suggests that one can do this by adding appropriate source terms to the equations. We find that a slightly modified version of this works quite well.

Although upwind schemes are generally very good at shock capturing, they can suffer from a non-linear instability if the flow is very closely aligned with the grid (Quirk 1994). They also tend to generate long wave entropy errors behind shocks which are moving slowly relative to the grid. In Falle & Komissarov (1996) we showed that these problems can be eliminated by adding appropriate viscous fluxes to those computed from the solution to the Riemann problem. We find that this also considerably improves the performance of our MHD code.

2 THE MHD RIEMANN PROBLEM

In cartesian coordinates, the equations of ideal MHD can be written

in the conservative form (Brio & Wu 1988)

$$\frac{\partial \boldsymbol{U}}{\partial t}+\frac{\partial \boldsymbol{F}}{\partial x}+\frac{\partial \boldsymbol{G}}{\partial y}+\frac{\partial \boldsymbol{H}}{\partial z}=0,$$

where

$$\boldsymbol{U}=[\rho, \rho v_x, \rho v_y, \rho v_z, e, B_x, B_y, B_z]^{\mathrm{t}} \tag{1}$$

is a vector of conserved variables. Here t denotes the transpose and

$$e=\frac{p_{\mathrm{g}}}{(\gamma-1)}+\frac{1}{2}B^2+\frac{1}{2}\rho v^2$$

is the total energy per unit volume. p_{g} is the gas pressure.

The fluxes are given by

$$\boldsymbol{F}=\begin{bmatrix} \rho v_x \\ \rho v_x^2+p_{\mathrm{g}}+p_{\mathrm{m}}-B_x^2 \\ \rho v_x v_y-B_xB_y \\ \rho v_x v_z-B_xB_z \\ \{e+p_{\mathrm{g}}+p_{\mathrm{m}}\}v_x-B_x(\boldsymbol{v}\cdot\boldsymbol{B}) \\ 0 \\ v_xB_y-v_yB_x \\ v_xB_z-v_zB_x \end{bmatrix}, \tag{2}$$

$$\boldsymbol{G}=\begin{bmatrix} \rho v_y \\ \rho v_y v_x-B_yB_x \\ \rho v_y^2+p_{\mathrm{g}}+p_{\mathrm{m}}-B_y^2 \\ \rho v_y v_z-B_yB_z \\ \{e+p_{\mathrm{g}}+p_{\mathrm{m}}\}v_y-B_y(\boldsymbol{v}\cdot\boldsymbol{B}) \\ v_yB_x-v_xB_y \\ 0 \\ v_yB_z-v_zB_y \end{bmatrix}, \tag{3}$$

$$\boldsymbol{H}=\begin{bmatrix} \rho v_z \\ \rho v_z v_x-B_zB_x \\ \rho v_z v_y-B_zB_y \\ \rho v_z^2+p_{\mathrm{g}}+p_{\mathrm{m}}-B_z^2 \\ \{e+p_{\mathrm{g}}+p_{\mathrm{m}}\}v_z-B_z(\boldsymbol{v}\cdot\boldsymbol{B}) \\ v_zB_x-v_xB_z \\ v_zB_y-v_yB_z \\ 0 \end{bmatrix} \tag{4}$$

where

$$p_{\mathrm{m}}=\frac{1}{2}B^2$$

is the magnetic pressure. The units in these equations are such that the velocity of light and the factor 4π do not appear.

The Riemann problem is governed by the one dimensional version of these equations

$$\frac{\partial \boldsymbol{U}}{\partial t}+\frac{\partial \boldsymbol{F}}{\partial x}=0. \tag{5}$$

Although other authors have used the conserved variables, it is more convenient to solve the linear Riemann problem in terms of the primitive variables

$$\boldsymbol{P}=[\rho, v_x, v_y, v_z, p_{\mathrm{g}}, B_y, B_z]^t.$$

These satisfy

$$\frac{\partial \boldsymbol{P}}{\partial t}+\mathbf{A}\frac{\partial \boldsymbol{P}}{\partial x}=0$$

where the matrix $\mathbf{A}$ is given by

$$\mathbf{A}=\begin{bmatrix} v_x & \rho & 0 & 0 & 0 & 0 & 0 \\ 0 & v_x & 0 & 0 & \frac{1}{\rho} & \frac{B_y}{\rho} & \frac{B_z}{\rho} \\ 0 & 0 & v_x & 0 & 0 & -\frac{B_x}{\rho} & 0 \\ 0 & 0 & 0 & v_x & 0 & 0 & -\frac{B_x}{\rho} \\ 0 & \rho a^2 & 0 & 0 & v_x & 0 & 0 \\ 0 & B_y & -B_x & 0 & 0 & v_x & 0 \\ 0 & B_z & 0 & -B_x & 0 & 0 & v_x \end{bmatrix}.$$

Here a is the adiabatic sound speed

$$a=(\gamma p_{\mathrm{g}}/\rho)^{1/2}.$$

This system of equations only has seven variables since the condition $\nabla\cdot\boldsymbol{B}=0$ requires that the x component of the magnetic field must be constant if there is no y or z dependence. There are therefore seven waves whose speeds are given by the eigenvalues of $\mathbf{A}$. These are

$$\lambda_{1,7}=v\mp c_{\mathrm{f}}, \lambda_{2,6}=v\mp c_{\mathrm{a}}, \lambda_{3,5}=v\mp c_{\mathrm{s}}, \lambda_4=v,$$

where

$$c_{\mathrm{a}}=|B_x|/\sqrt{\rho}$$

is the Alfvén speed and

$$c_{\mathrm{s,f}}^2=\frac{1}{2}\left\{a^2+\frac{B^2}{\rho}\mp\left[\left(a^2+\frac{B^2}{\rho}\right)^2-\frac{4a^2B_x^2}{\rho}\right]^{1/2}\right\}$$

are the slow and fast magnetosonic speeds. Note that we have labelled these so that $\lambda_1\le\lambda_2\le\ldots\lambda_7$.

The right eigenvectors corresponding to these are

$$\begin{aligned} \boldsymbol{r}_{1,7}&=\left[\rho, \mp c_{\mathrm{f}}, \pm\frac{c_{\mathrm{f}}B_x\boldsymbol{B}_{\mathrm{t}}}{\Delta_{\mathrm{f}}}, \rho a^2, \frac{\rho c_{\mathrm{f}}^2\boldsymbol{B}_{\mathrm{t}}}{\Delta_{\mathrm{f}}},\right]^{\mathrm{t}}, \\ \boldsymbol{r}_{2,6}&=[0, 0, sB_z, -sB_y, 0, \pm B_z\sqrt{\rho}, \mp B_y\sqrt{\rho}]^{\mathrm{t}}, \\ \boldsymbol{r}_{3,5}&=\left[\rho, \mp c_{\mathrm{s}}, \pm\frac{c_{\mathrm{s}}B_x\boldsymbol{B}_{\mathrm{t}}}{\Delta_{\mathrm{s}}}, \rho a^2, \frac{\rho c_{\mathrm{s}}^2\boldsymbol{B}_{\mathrm{t}}}{\Delta_{\mathrm{s}}}\right]^{\mathrm{t}}, \\ \boldsymbol{r}_4&=[1, 0, 0, 0, 0, 0, 0]^t, \end{aligned} \tag{6}$$

where

$$s=\mathrm{sign}(B_x), \quad \Delta_{\mathrm{s,f}}=\rho c_{\mathrm{s,f}}^2-B_x^2.$$

and $\boldsymbol{B}_{\mathrm{t}}$ is the transverse magnetic field.

Although not strictly necessary, it is also useful to determine the left eigenvectors

$$\begin{aligned} \boldsymbol{l}_{1,7}&=\left[0, \mp c_{\mathrm{f}}, \pm\frac{c_{\mathrm{f}}B_x\boldsymbol{B}_{\mathrm{t}}}{\Delta_{\mathrm{f}}}, \frac{1}{\rho}, \frac{c_{\mathrm{f}}^2\boldsymbol{B}_{\mathrm{t}}}{\Delta_{\mathrm{f}}}\right], \\ \boldsymbol{l}_{2,6}&=\left[0, 0, sB_z, -sB_y, 0, \pm\frac{B_z}{\sqrt{\rho}}, \mp\frac{B_y}{\sqrt{\rho}}\right], \\ \boldsymbol{l}_{3,5}&=\left[0, \mp c_{\mathrm{s}}, \pm\frac{c_{\mathrm{s}}B_x\boldsymbol{B}_{\mathrm{t}}}{\Delta_{\mathrm{s}}}, \frac{1}{\rho}, \frac{c_{\mathrm{s}}^2\boldsymbol{B}_{\mathrm{t}}}{\Delta_{\mathrm{s}}}\right], \\ \boldsymbol{l}_4&=[1, 0, 0, 0, -1/a^2, 0, 0]. \end{aligned}$$

It convenient to normalize these so that

$$\boldsymbol{l}_i\cdot\boldsymbol{r}_j=\delta_{ij}.$$

This can obviously be done by multiplying the left and right eigenvectors by appropriate factors. However, one has to be rather careful how one does this since otherwise the eigenvectors corresponding to the Alfvén waves and two of the magnetosonic waves are not well-defined when the transverse component of the magnetic field vanishes (Brio & Wu 1988).

For the Alfvén waves we have

$$\boldsymbol{l}_{2,6}\cdot\boldsymbol{r}_{2,6} = 2(B_y^2 + B_z^2) = 2B_\mathrm{t}^2$$

where B_t is the magnitude of the transverse magnetic field. The symmetry of the left and right eigenvectors suggests that we should multiply them both by

$$\alpha = 1/\sqrt{2}B_\mathrm{t}.$$

Apart from the factor $\sqrt{2}$, this is the same as the normalization that Brio & Wu derived without considering the left eigenvectors. If we use this, then the non-zero components of both the left and right eigenvectors are proportional to B_y/B_t and B_z/B_t. These remain finite as $B_\mathrm{t}\rightarrow 0$, but are undetermined unless we specify the direction of the tranverse field as it tends to zero. We therefore need to show that, whatever direction we choose, the eigenvectors remain linearly independent when $B_\mathrm{t} = 0$. In order to do this we have to consider the behaviour of the magnetosonic waves when the transverse field vanishes.

For the magnetosonic waves we have

$$\boldsymbol{l}_{\mathrm{s,f}}\cdot\boldsymbol{r}_{\mathrm{s,f}} = 2c_{\mathrm{s,f}}^2\left[1 + \frac{B_x^2 B_\mathrm{t}^2}{\Delta_{\mathrm{s,f}}^2}\right].$$

As for the Alfvén waves, the form of the eigenvectors suggests that we normalize them by multiplying both left and right eigenvectors by

$$\beta_{\mathrm{s,f}} = \frac{1}{(\boldsymbol{l}_{\mathrm{s,f}}\cdot\boldsymbol{r}_{\mathrm{s,f}})^{1/2}} = \frac{\Delta_{\mathrm{s,f}}}{\sqrt{2}c_{\mathrm{s,f}}(\Delta_{\mathrm{s,f}}^2 + B_x^2 B_\mathrm{t}^2)^{1/2}}.$$

Although this normalization is different from that adopted by Brio & Wu (1988), it is entirely equivalent and seems somewhat more natural. When $B_\mathrm{t} = 0$ we have $c_\mathrm{s} = c_\mathrm{a}$ if $c_\mathrm{a} < a$, whereas $c_\mathrm{f} = c_\mathrm{a}$ if $c_\mathrm{a} > a$. We therefore have slow-wave degeneracy at $B_\mathrm{t} = 0$ ($\Delta_\mathrm{s} = 0$) if $c_\mathrm{a} < a$ and fast-wave degeneracy ($\Delta_\mathrm{f} = 0$) if $c_\mathrm{a} > a$.

First suppose that the slow waves are degenerate ($c_\mathrm{a} < a$). Then

$$\Delta_\mathrm{s} \rightarrow -\frac{B_\mathrm{t}^2 B_x^2}{\rho(a^2 - c_\mathrm{a}^2)} \text{ as } B_\mathrm{t}\rightarrow 0,$$

which means that

$$\beta_\mathrm{s} \rightarrow \frac{\Delta_\mathrm{s}}{\sqrt{2}B_x B_\mathrm{t} c_\mathrm{s}} \text{ as } B_\mathrm{t}\rightarrow 0.$$

The normalized slow-wave eigenvectors therefore also have components which are proportional to B_y/B_t and B_z/B_t as $B_\mathrm{t}\rightarrow 0$. It is easy to show that, although the Alfvén waves and the slow waves have the same wavespeed when $B_\mathrm{t} = 0$, the corresponding eigenvectors are linearly independent whatever the direction of the transverse field as it tends to zero.

If the fast waves are degenerate ($c_\mathrm{a} > a$), then

$$\Delta_\mathrm{f} \rightarrow \frac{B_\mathrm{t}^2 B_x^2}{\rho(c_\mathrm{a}^2 - a^2)} \text{ as } B_\mathrm{t}\rightarrow 0,$$

so that, apart from the change of sign, the fast waves behave in the same way as the slow waves do when $c_\mathrm{a} < a$.

Finally, if both sets of waves are degenerate ($c_\mathrm{a} = a$), we have

$$\Delta_{\mathrm{s,f}} \rightarrow \mp 2aB_\mathrm{t}\sqrt{\rho} \text{ as } B_\mathrm{t}\rightarrow 0.$$

and

$$\beta_{\mathrm{s,f}} \rightarrow \left(\frac{2}{5}\right)^{1/2}\frac{1}{c_\mathrm{a}} \text{ as } B_\mathrm{t}\rightarrow 0.$$

The normalized eigenvectors still contain components proportional to B_y/B_t and B_z/B_t as $B_\mathrm{t}\rightarrow 0$. Note that although the Alfvén, fast and slow speeds now become identical when $B_\mathrm{t} = 0$, the corresponding eigenvectors are still linearly independent provided we assume that $\Delta_\mathrm{s}\rightarrow 0^-$ and $\Delta_\mathrm{f}\rightarrow 0^+$ as $B_\mathrm{t}\rightarrow 0$.

When $B_x = 0$, things become very simple. The fast waves are no longer able to change the transverse velocity and the slow and Alfvén waves merge with the contact discontinuity. The equations reduce to those of ordinary gas dynamics with a total pressure given by $P = p_\mathrm{g} + p_\mathrm{m}$. The magnetic field is determined by the condition that $\boldsymbol{B}_\mathrm{t}/\rho$ for each fluid particle be independent of time. In this case nothing special happens when $B_\mathrm{t}\rightarrow 0$.

The solution to the one dimensional Riemann problem satisfies (5) with the initial conditions

$$\begin{aligned}\boldsymbol{U}(x,0) &= \text{constant} = \boldsymbol{U}_\mathrm{R} \text{ for } x \geq 0,\\ \boldsymbol{U}(x,0) &= \text{constant} = \boldsymbol{U}_\mathrm{L} \text{ for } x < 0.\end{aligned}$$

Since there is no length-scale in the problem, the solution must have the self-similar form $\boldsymbol{U}(x,t) = \boldsymbol{U}(x/t)$ and can therefore only contain contact discontinuities, Alfvén shocks, and magnetosonic shocks or centred rarefactions. As in ordinary gas dynamics, the solution cannot be found explicitly but has to be determined from a set of non-linear algebraic equations. As we have already pointed out, one could use the exact solver in a numerical scheme since, although it is expensive, it is only needed for the small number of Riemann problems for which there is a large difference between the left and right states. However, as we shall see, a simple linear Riemann solver works just as well for everything apart from strong rarefactions.

2.1 Approximate solutions to the Riemann problem

The simplest way of constructing an approximate solution is to solve the linear problem

$$\frac{\partial \boldsymbol{P}}{\partial t} + \overline{\mathbf{A}}\frac{\partial \boldsymbol{P}}{\partial x} = 0$$

where $\overline{\mathbf{A}}(\boldsymbol{P}_\mathrm{L}, \boldsymbol{P}_\mathrm{R})$ is some mean matrix.

For some systems, such as classical gas dynamics, it is easy to construct a mean matrix with the property (Roe 1981)

$$\boldsymbol{F}(\boldsymbol{U}_\mathrm{R}) - \boldsymbol{F}(\boldsymbol{U}_\mathrm{L}) = \overline{\mathbf{A}}(\boldsymbol{U}_\mathrm{R} - \boldsymbol{U}_\mathrm{L}), \tag{7}$$

which ensures that the solution to the Riemann problem is exact for a single shock. Brio & Wu (1988) showed that such a matrix does not have a simple form in MHD unless $\gamma = 2$, but this does not matter much since it is not shocks, but rarefactions, which cause problems for approximate Riemann solvers.

In fact both Brio & Wu (1988) and Ryu & Jones (1995) found that

$$\overline{\mathbf{A}}(\boldsymbol{P}_\mathrm{L}, \boldsymbol{P}_\mathrm{R}) = \mathbf{A}\left[\frac{1}{2}(\boldsymbol{P}_\mathrm{L} + \boldsymbol{P}_\mathrm{R})\right] \tag{8}$$

works just as well as one which satisfies (7).

Whatever mean matrix one chooses, the state at $x = 0$ is given by

$$\begin{aligned}\boldsymbol{P}^* &= \boldsymbol{P}_\mathrm{L} + \sum_{\overline{\lambda}_i<0}\frac{\overline{\boldsymbol{l}}_i\cdot(\boldsymbol{P}_\mathrm{R} - \boldsymbol{P}_\mathrm{L})}{(\overline{\boldsymbol{l}}_i\cdot\overline{\boldsymbol{r}}_i)}\\ &= \boldsymbol{P}_\mathrm{R} - \sum_{\overline{\lambda}_i>0}\frac{\overline{\boldsymbol{l}}_i\cdot(\boldsymbol{P}_\mathrm{R} - \boldsymbol{P}_\mathrm{L})}{(\overline{\boldsymbol{l}}_i\cdot\overline{\boldsymbol{r}}_i)}\end{aligned}$$

where $\overline{\lambda}_i, \overline{\boldsymbol{r}}_i, \overline{\boldsymbol{l}}_i$ are the eigenvalues and eigenvectors of $\overline{\mathbf{A}}$.

As we have already pointed out, something special has to be done when $B_t = 0$ in $\overline{\mathbf{A}}$. Brio & Wu use the limiting forms of the eigenvectors with $B_y/B_t \to 1/\sqrt{2}$, $B_z/B_t \to 1/\sqrt{2}$ as $B_t \to 0$, but since the field directions in the exact solution to the Riemann problem are determined by those in the left and right states, it might seem sensible to do something similar in the approximate solution. However, we find that not only does the choice of field direction make no detectable difference to the numerical solution, but one can get away with using ordinary gas dynamics when $B_t = 0$ in $\overline{\mathbf{A}}$. This simply amounts to ignoring the Alfvén waves and the degenerate magnetosonic waves and supposing that the remaining magnetosonic waves do not change the transverse components of either the field or velocity. Although this is clearly a very drastic approximation, it is not really any worse than imposing an arbitrary field direction on the degenerate waves. It certainly seems to work just as well and is a great deal simpler.

It is possible to avoid using a mean matrix by supposing that $\mathbf{A} = \mathbf{A}^{\rm L} = \mathbf{A}(\boldsymbol{P}_{\rm L})$ on the left of the contact discontinuity and $\mathbf{A} = \mathbf{A}^{\rm R} = \mathbf{A}(\boldsymbol{P}_{\rm R})$ on the right. Let us denote the eigenvalues and eigenvectors of these matrices by the superfixes L and R. Then if $\boldsymbol{P}^*_{\rm L}$ and $\boldsymbol{P}^*_{\rm R}$ are the states on either side of the contact discontinuity, we have

$$\boldsymbol{P}^*_{\rm L} = \boldsymbol{P}_{\rm L} + \sum_{i=1}^{3} b_i \boldsymbol{r}^{\rm L}_i,$$

$$\boldsymbol{P}^*_{\rm R} = \boldsymbol{P}_{\rm R} + \sum_{i=5}^{7} b_i \boldsymbol{r}^{\rm R}_i.$$

We have excluded the contact discontinuity, so there must be exactly six coefficients b_i in these equations. At the contact discontinuity we have

$$\boldsymbol{v}^*_{\rm L} = \boldsymbol{v}^*_{\rm R}, \boldsymbol{B}^*_{\rm L} = \boldsymbol{B}^*_{\rm R}, p^*_{\rm L} = p^*_{\rm R}.$$

Since the x component of the magnetic field is constant, these conditions are sufficient to determine the six coefficients b_i. If the transverse magnetic field is zero in either the left or the right state, then we can use ordinary gas dynamics on that side, just as before.

In Falle & Komissarov (1996) we called the approximation that uses the mean matrix defined by equation (8) Riemann solver A, and the one with two matrices Riemann solver B. We found that B was much better for relativistic flows than A, but in classical gas dynamics or MHD there appears to be very little difference between them. If this is always true, then A is clearly better since it is somewhat cheaper than B.

2.2 The exact solution to the Riemann problem

As we have already pointed out, although a linear solver is perfectly adequate for the great majority of the Riemann problems that occur in a numerical calculation, it is possible for a linear solver to generate unphysical negative pressures and/or densities if strong rarefaction waves are present. One remedy to fix such solutions by setting the pressure and density to the prescribed floor values, but it is known that in pure gas dynamics this does not always help. In such cases it is much safer to use an exact Riemann solver.

Linear solutions of MHD Riemann problems may also include magnetosonic waves (both shocks and rarefactions) which change the sign of the tangential component of magnetic field i.e. non-evolutionary solutions. One might suppose that it is these that give rise to the intermediate shock in the numerical solution of Brio & Wu problem and hope that an exact Rieman solver can cure this. As we shall see in Section 5, this is a vain hope, but we still need an exact Riemann solver which excludes intermediate waves in order to test our numerical solutions.

The larger number of waves and the various degenerate cases make the Riemann problem much more complicated for MHD than it is for pure gas dynamics. This is presumably why there have, as yet, only been a couple of attempts to construct a numerical algorithm for this problem. Dai & Woodward (1994) describe a technique in which shocks, Alvfén waves and contact discontinuities are treated exactly, but rarefactions are approximated by rarefaction shocks. Obviously, such a method only gives good results for problems with weak rarefactions. Ryu & Jones (1995) have devised an improved version in which rarefactions are treated correctly. However, they found that it does not converge in the cases involving switch-on or switch-off waves. In this section we describe a different exact Riemann solver, which seems to be robust.

2.2.1 *Parameter space*

Our first task is to decide upon a suitable set of parameters to describe the wave strengths. These parameters must obviously determine the strengths of all permitted waves uniquely, but it is very convenient if they also have a known finite range for all physically admissible waves.

Let the suffices $1 \ldots 6$ denote the states between the waves ordered from left to right. The Alfvén waves are the only ones that can affect the angle

$$\theta = \tan^{-1}(B_y/B_z),$$

that the transverse field makes with the y-axis. Since this angle must be the same on both sides of the contact discontinuity, we must have $\theta_3 = \theta_4 = \theta_{\rm c}$. Hence

$$Q_{\rm a} = \theta_{\rm c}/2\pi$$

lies in $[0, 1)$ and uniquely determines the strengths of both Alfvén waves.

Unfortunately, it is not so easy to find appropriate parameters for magnetosonic waves. Both Dai & Woodward (1995) and Ryu & Jones (1995) used the magnitudes of the transverse field,

$$B_{\rm t} = (B_y^2 + B_z^2)^{1/2},$$

in the states $\boldsymbol{P}_1$, $\boldsymbol{P}_3$, and $\boldsymbol{P}_6$ as the other parameters. Since $B_{\rm t3} = B_{\rm t4}$ this provides one post-wave variable for each of the magnetosonic waves and would therefore appear to be sufficient to determine their strengths. However, this choice has several disadvantages. First, it is obviously no good for pure gasdynamic waves for which $B_{\rm t} = 0$. Secondly, the jump in $B_{\rm t}$ does not always determine fast shocks uniquely (Jeffreys & Taniuti 1964; Kulikovskiy & Lyubimov 1965). Finally, there is a maximum possible variation of $B_{\rm t}$ in slow rarefactions, which corresponds to cavitation. Thus, an arbitrarily chosen value of $B_{\rm t}$ in the state behind the slow wave may well fall in a prohibited range. Unfortunately, the permitted range of $B_{\rm t}$ behind the slow wave in a Riemann problem is not known a priori, but depends on the strength of the fast wave that precedes it.

We therefore choose to describe the strengths of magnetosonic waves in a somewhat different way. The left fast wave (shock or rarefaction) is described by the parameter

$$Q_{\rm fL} = [\rho_1 - \rho_{\rm min}(\boldsymbol{P}_{\rm L})]/[(\rho_{\rm max}(\boldsymbol{P}_{\rm L}) - \rho_{\rm min}(\boldsymbol{P}_{\rm L})],$$

where $\rho_{\rm min}(\boldsymbol{P})$ is the minimum density that can be attained in a fast rarefaction and $\rho_{\rm max}(\boldsymbol{P})$ is the maximum density that can be attained in a fast shock with upstream state $\boldsymbol{P}$. We can define an analogous parameter , $Q_{\rm fR}$, for the right fast wave. The permitted range for these is obviously $[0, 1)$. Given $Q_{\rm fL}$ one can compute ρ_1, decide

whether the wave is a shock ($\rho_1 > \rho_L$) or rarefaction ($\rho_1 < \rho_L$), and then compute $\boldsymbol{P}_1$.

We cannot do quite the same thing for slow waves since the downstream density does not determine the slow shock uniquely (Jeffreys & Taniuti 1964). Instead, we use

$$Q_{sL} = \rho_3/\rho_{so}(\boldsymbol{P}),$$

where $\rho_{so}(\boldsymbol{P})$ is the density downstream of a switch-off shock with upstream state $\boldsymbol{P}$. Since the density can fall to zero in a slow rarefaction, the permitted range of Q_{sL} is (0, 1]. Given $\boldsymbol{P_2}$ and Q_{sL} one can compute $\rho_{so}(\boldsymbol{P_2})$ and hence ρ_3. If $\rho_3 < \rho_2$, then the wave is a rarefaction and we can safely use ρ_3 to compute the downstream state, $\boldsymbol{P}_3$. However, if $\rho_3 > \rho_2$ then the wave is a slow shock and ρ_3 should not be regarded as the density in the downstream state. Instead we simply use it to calculate the shock speed, $\tilde{u}_s$, relative to the upstream state from

$$\tilde{u}_s = c_s + (c_a - c_s) * \frac{\rho_3 - \rho_2}{\rho_{so} - \rho_2},$$

where c_s, c_a correspond to the upstream state, $\boldsymbol{P}_2$. $\tilde{u}_s$ can then be used to determine the downstream state uniquely. Exactly the same thing can be done for the right slow wave.

The five parameters, $\boldsymbol{Q} = (Q_a, Q_{fL}, Q_{fR}, Q_{sL}, Q_{sR})$, clearly determine the wave strengths uniquely and all lie in the interval [0, 1) for physically admissible waves. Given these, we can compute the states $\boldsymbol{P}_3$ and $\boldsymbol{P}_4$ on either side of the contact discontinuity (in section 2.1 these were called $\boldsymbol{P}_L^*$ and $\boldsymbol{P}_R^*$ respectively). They have to satisfy

$$\begin{aligned} B_{t_3}(Q_{fL}, Q_{sL}) &= B_{t_4}(Q_{fR}, Q_{sR}), \\ \boldsymbol{v}_3(Q_{fL}, Q_a, Q_{sL}) &= \boldsymbol{v}_4(Q_{fR}, Q_a, Q_{sR}), \\ p_{g_3}(Q_{fL}, Q_{sL}) &= p_{g_4}(Q_{fR}, Q_{sR}), \end{aligned} \tag{9}$$

which gives five equations to determine the five wave strengths. We solve these by iteration using the Newton–Raphson technique.

In order to compute $\boldsymbol{P}_3$ and $\boldsymbol{P}_4$ one has to be able to determine the jumps across fast and slow shocks and fast and slow rarefactions from the above parameters.

2.2.2 *Solution of the shock equations*

For fast shocks we use the downstream density as a parameter, in which case the shock equations reduce to a cubic equation for the jump in the magnetic field

$$h^3 + a_2 h^2 + a_1 h + a_0 = 0, \tag{10}$$

where

$$\begin{aligned} a_2 &= \sin\Theta_0(2 - \gamma\eta), \\ a_1 &= \eta\left[(\gamma - 1)\eta + 2(s_0 - 1)\right], \\ a_0 &= -2s_0 \sin\Theta_0 \eta^2. \end{aligned}$$

Here we have adopted the notation of Jeffreys & Taniuti (1964)

$$\eta = \frac{[\rho]}{\rho_0}, \quad h = \frac{[B_y]}{B_0},$$

$$B_0^2 = B_x^2 + B_{y_0}^2, \quad \sin\Theta_0 = B_{y_0}/B_0, \quad s_0 = \gamma p_{g_0}/B_0^2,$$

The suffix 0 indicates the upstream state and we have chosen a reference frame in which $B_{z_0} = 0$ and $B_{y_0} > 0$.
The fast shock solution of (10) is the one which gives the maximum increase in B_y. The other variables in the downstream state can then be found from

$$[p_g] = \left(\frac{1}{4}\eta[B_y]^2 + \frac{\gamma}{\gamma - 1} p_{g_0}\eta\right)\left(\frac{1}{\gamma - 1} - \frac{1}{2}\eta\right)^{-1}, \tag{11}$$

$$G^2 = -\frac{1}{[\tau]}\left([p_g] + \frac{1}{2}[B_y]^2 + B_{y_0}[B_y])\right),$$

$$[u_z] = 0 \tag{12}$$

$$[u_y] = \frac{B_x}{G}[B_y], \tag{13}$$

in which $\tau = 1/\rho$ is the specific volume and G

$$G = \rho_0(u_{x_0} - u_s)$$

is the mass flux through the shock. u_s is the shock speed in the laboratory frame.

As we have already pointed out, we cannot use the downstream density as a parameter for slow shocks since it does not determine the shock uniquely. Instead we use the shock speed relative to the upstream state, $\tilde{u}_{s_0}$. Then if $B_{y_0} \neq 0$, the shock equations reduce to a fourth-order equation for τ (Cabannes 1970)

$$\begin{aligned} (\tau - \tau_*)^2 &\left(2K - \frac{2\gamma}{\gamma - 1} F_n \tau + \frac{\gamma + 1}{\gamma - 1} G^2 \tau^2\right) \\ &+ F_t^2 \left(\frac{\tau}{\tau_*}\right)\left(\frac{\gamma}{\gamma - 1}\tau_* - \tau\right) = 0, \end{aligned} \tag{14}$$

where F_n, F_t, and K are the other shock invariants

$$F_n = G^2\tau + p_g + \frac{B_y^2}{2}, \tag{15}$$

$$F_t = B_y(\tau - \tau_*) \tag{16}$$

$$K = \frac{\gamma}{\gamma - 1}\tau p_g + \frac{1}{2}G^2\tau^2\left(1 + \frac{B_y^2}{B_x^2}\right), \tag{17}$$

$$\tau_* = B_x^2/G^2.$$

Once (15) has been solved for τ, the other downstream variables can be found from (15–17) and (12,13). The slow shock solution is selected by using the conditions $B_y < B_{y_0}$, $B_y \geq 0$.

If $B_{y_0} = 0$, then instead of (15) one obtains

$$2K - \frac{2\gamma}{\gamma - 1} F_n \tau + \frac{\gamma + 1}{\gamma - 1} G^2\tau^2 = 0,$$

which has the two solutions

$$\tau_1 = \tau_0,$$

$$\tau_2 = \tau_0\left(\frac{\gamma - 1}{\gamma + 1} + \frac{2}{\gamma + 1}\frac{a_0^2}{\tilde{u}_{s_0}^2}\right). \tag{18}$$

Jeffreys & Taniuti (1964, p. 247) suggest that the slow shock vanishes as $B_{y_0}/B_x \to 0$, but this is not quite true. From (18) one can see that $\tau_2 < \tau_0$ only if $\tilde{u}_{s_0} > a_0$. Therefore, if $a_0 > c_{a_0}$, then τ_1 is indeed the only acceptable solution for slow shock. However, if $a_0 < c_{a_0}$ then τ_2 is also acceptable. In this case the slow shock does not vanish but tends to a pure gas dynamic shock. The maximum compression ratio of such a limiting shock is determined by the condition $\tilde{u}_{s_0} = c_{a_0}$ and is equal to

$$\left(\frac{\rho_2}{\rho_0}\right)_{max} = \frac{\gamma + 1}{\gamma - 1 + 2(a_0/c_{x_0})^2}$$

For higher values of $\tilde{u}_{s_0}$, this pure gas shock first turns into a limiting intermediate shock and then into a limiting fast shock. This explains the division of the shock diagram in Jeffreys & Taniuti (1964,

fig. 6.9b) into the X, Y, and Z regions (a similar analysis is given in Kulikovskiy & Lyubimov 1965).

2.2.3 *Rarefactions*

Rarefactions are described by the following system of ordinary differential equations

$$\frac{\mathrm{d}\boldsymbol{P}}{\mathrm{d}\mu} = \boldsymbol{r}_k \tag{19}$$

where μ is some variable parameter and r_k is one of the right eigenvectors given by equations (6) with $k = 1, 3, 5$ or 7.

As before, we use the suffix 0 to indicate the upstream state, and choose a reference frame in which $B_{z0} = 0, B_{y0} > 0$. From (19) it is easy to show that

$$u_z = u_{z0}, \qquad p_\mathrm{g} = p g_0 (\rho / \rho_0)^\gamma. \tag{20}$$

It is convenient to introduce the variables $\alpha = c_{\mathrm{s,f}}^2 / a^2$ and $\beta = a^2 / {c_\mathrm{a}}^2$. These are related by

$$\frac{\mathrm{d}\alpha}{\mathrm{d}\beta} = \frac{2-\gamma}{\gamma}\left[\frac{\alpha^2(\alpha-1)}{\alpha^2\beta - 1}\right]. \tag{21}$$

(Jeffreys & Taniuti 1964). In terms of these we get

$$\rho = \rho_0 (\beta/\beta_0)^{1/\gamma}, \tag{22}$$

$${B_y}^2 = {B_x}^2 \frac{(\alpha-1)(\beta\alpha - 1)}{\alpha}. \tag{23}$$

The minimum density $\rho_{\min}$ that can be attained via a fast rarefaction occurs in a switch-off rarefaction and corresponds to $\alpha\beta = 1$. Therefore, in order to find $\rho_{\min}$ it is convenient to define a new variable, $\xi = \alpha\beta$. Equation (21) can then be written

$$\frac{\mathrm{d}\beta}{\mathrm{d}\xi} = \gamma \frac{\beta(\xi^2 - \beta)}{\xi[2\xi(\xi-\beta) + \gamma\beta(\xi - 1)]}. \tag{24}$$

Integrating this equation from $\xi = \xi_0$ to $\xi = 1$ gives $\beta_{\min}$, which can be used in 22 to get $\rho_{\min}$.

Given the density downstream of the rarefaction wave, the other variables can be found as follows: p_g, u_z, and β are obtained from equations (20,22); equation (21) is then integrated to get α, which allows us to compute B_y from equation (23); finally u_x and u_y are obtained by a numerical integration of the appropriate components of the system (19).

The numerical integration of equations (21,24) presents no problems, except near the critical point $(\alpha, \beta) = (1, 1)$ where we need to use an approximate analytic solution. We can use $\mu = \rho$ in (19) unless the tangential field becomes small ($\alpha\beta - 1 \ll 1$), in which case it is better to put $\mu = B_y$.

2.2.4 *Degeneracies*

There are two degenerate types of MHD Riemann problems that require special treatment. If $B_x = 0$, then the slow and Alfvén waves merge with the contact discontinuity. We deal with this by ignoring the slow and Alfvén waves when $B_x^2 / (\rho c_\mathrm{f}^2)$ is small enough for rounding errors to be important.

Another kind of degeneracy occurs when the solution to the Riemann problem has vanishing tangential component of the magnetic field in the states 1 and 6. In this case all derivatives with respect to Q_a vanish and the Jacobian of (9) becomes singular. If this degeneracy is detected, then we eliminate Q_a from the list of unknowns and reduce the number of equations in (9) by combining the equations for v_y and v_z. As in the previous case, we have to switch to this procedure when the tangential magnetic field becomes small enough for rounding errors to be significant.

Although this method of dealing with degeneracies makes the Riemann solver robust when it is used in a numerical scheme, it does mean that our solution is not exact for such cases. However, we can get so close to the degenerate limit by using the asymptotic expressions for the wavespeeds and components of the eigenvectors, that there seems to be little point in trying to devise a more elaborate procedure.

Since the linear solutions of the nonlinear Riemann problems are not particulary close to the exact ones and may even be unphysical,, there is not much point in using them as an initial guess for the Newton–Raphson iterations. Instead our initial guess is obtained by ignoring the magnetosonic waves and setting $\theta_\mathrm{c} = 0.5(\theta_\mathrm{L} + \theta_\mathrm{R})$. Surprisingly, this converges for all the test problems in Dai & Woodward (1994) as well as the ones in the present paper. In fact we have not yet been able to find a case for which our procedure fails.

3 NUMERICAL MAGNETIC MONOPOLES

Although the exact equations ensure $\nabla\cdot\boldsymbol{B} = 0$ remains true if it is so initially, a numerical scheme does not automatically do this. Brackbill & Barnes (1980) have shown that a conservative numerical scheme which does not enforce $\nabla\cdot\boldsymbol{B} = 0$ misbehaves in regions where the other forces are close to equilibrium. We also find that if we do not do anything about $\nabla\cdot\boldsymbol{B} = 0$, then our scheme fails in more than one dimension if the initial state contains a discontinuity in the magnetic field. The reason for this is that, although the scheme maintains $\nabla\cdot\boldsymbol{B} = 0$ to truncation error, these errors are $O(1)$ at discontinuities. The effect of this is to introduce a significant density of numerical monopoles at discontinuities which then wreak havoc with the solution.

There are a number of ways of dealing with this. It is possible to enforce $\nabla\cdot\boldsymbol{B} = 0$ exactly by working with the the integral form of the induction equation, but, as Zachary et al. (1994) have pointed out, this requires a staggered grid. They therefore ensured a divergence free magnetic field by solving a Poisson equation for a pseudo-potential and then using this to correct the field. Since this is clearly quite expensive, it is worth asking if it is really necessary.

There are really two aspects to this problem. The first is that a divergence-free field has certain topological properties. If these are crucial to the problem, then it might seem that one has no choice but to enforce $\nabla\cdot\boldsymbol{B} = 0$ exactly. However, all numerical schemes have a finite resistivity, which means that the topological properties of the field are in any case not as they would be for a perfectly conducting fluid. It is therefore not at all obvious that it is worth going to the trouble of correcting the field to make it divergence free. Indeed, Zachary et al. found that it made no discernible difference to their results. The other effects are much more serious. These arise because, if $\nabla\cdot\boldsymbol{B} \neq 0$, then the conservative forms of the equations contain terms that are not present in the non-conservative forms. It is these terms which are responsible for the bad behaviour of conservative schemes. Fortunately, this difficulty can be removed by simply modifying the conservative equations.

First consider the momentum equation. If $\nabla\cdot\boldsymbol{B}$ does not vanish, then conservative and non-conservative forms of this equation are no longer equivalent because the divergence of the momentum fluxes in the conservative form contains an extra term which is proportional to $\nabla\cdot\boldsymbol{B}$. We can, however, restore the equivalence between the two forms by adding a term to the conservative form which cancels with the offending term. If one does this, then the

conservative form of the momentum equation becomes

$$\frac{\partial \rho \boldsymbol{v}}{\partial t} + \nabla\cdot(\rho \boldsymbol{v}\boldsymbol{v} + P\mathbf{I} - \boldsymbol{B}\boldsymbol{B}) = -\boldsymbol{B}\nabla\cdot\boldsymbol{B}, \tag{25}$$

where $\mathbf{I}$ is the 3×3 unit tensor and $P = p_{\rm g} + p_{\rm m}$ is the total pressure.

We can think of the term on the right-hand side of this equation as a body force which balances the force resulting from the numerical monopoles. The presence of this extra force means that we must add the work that it does to the energy equation

$$\frac{\partial e}{\partial t} + \nabla\cdot[(e+P)\boldsymbol{v} - \boldsymbol{B}(\boldsymbol{v}\cdot\boldsymbol{B})] = -(\boldsymbol{v}\cdot\boldsymbol{B})\nabla\cdot\boldsymbol{B}. \tag{26}$$

Actually Zachary et al. (1994) did not just correct the field to ensure that $\nabla\cdot\boldsymbol{B} = 0$, they also used a non-conservative differencing of the troublesome terms in the momentum and energy equations. Since this is entirely equivalent to using equations (25) and (26), it is not surprising that their scheme works well even when they do not correct the field.

It is not obvious that one needs to anything to the induction equation, and indeed Zachary et al. left it unchanged. However, if one uses the product rule on the divergence term in the conservative form, then there is also a term proportional $\nabla\cdot\boldsymbol{B} = 0$ in this equation. We should therefore also add this term to the right-hand side of the equation. The result is

$$\frac{\partial \boldsymbol{B}}{\partial t} + \nabla\cdot(\boldsymbol{v}\boldsymbol{B} - \boldsymbol{B}\boldsymbol{v}) = -\boldsymbol{v}\nabla\cdot\boldsymbol{B}. \tag{27}$$

If we take the divergence of this we get

$$\frac{\partial \nabla\cdot\boldsymbol{B}}{\partial t} + \nabla\cdot(\boldsymbol{v}\nabla\cdot\boldsymbol{B}) = 0, \tag{28}$$

which tells us that $\boldsymbol{v}\nabla\cdot\boldsymbol{B}$ is the flux of magnetic monopoles. One can therefore regard the extra term in (27) as a monopole current, which has to be added to the induction equation in order to compensate for the motion of the numerical monopoles. Note that although the monopoles are advected away from where they are created, they are not destroyed.

Equations (25–27) could also have been obtained by insisting that the equations be Galilean invariant even when $\nabla\cdot\boldsymbol{B} \neq 0$. This is essentially the argument that Powell (1994) used to determine the extra terms, although what he actually did was to consider how the one-dimensional equations should be modified to allow eight waves instead of seven while maintaining Galilean invariance. Since equation (28) means that the quantity $\nabla\cdot\boldsymbol{B}/\rho$ is advected with the fluid velocity, he also included an extra wave in the Riemann solver. However, we find that this is not necessary.

Whatever argument that is used to obtain the extra terms, there is no dispute about what they should be. What is worrying is that these source terms are at their most important at shocks, which is precisely where we need exact conservation to ensure that the shock conditions are satisfied. We find that these terms can be dispensed with if we use a Poisson equation to correct the field, but since this also destroys conservation, it is not clear that it is any better.

4 NUMERICAL SCHEME

The properties of an upwind schemes does not just depend on the particular approximate solution to the Riemann problem, but also on the way in which these problems are set up and the fluxes computed from the solution. This is not the place to discuss the various possibilities, except to say that, as far as we are aware, all the upwind schemes for MHD that have so far appeared in the literature have used a Roe-type second-order scheme (Roe 1986). In such schemes the second-order fluxes are calculated by integrating the solution to the linear Riemann problem over a time step. In contrast to this, we use the second-order scheme described in Falle (1991) and Falle & Komissarov (1996). Although these papers contain a detailed description of the scheme, it is worth repeating the basic ideas here for the sake of completeness.

The equations for the conserved variables are

$$\frac{\partial \boldsymbol{U}}{\partial t} + \frac{\partial \boldsymbol{F}}{\partial x} + \frac{\partial \boldsymbol{G}}{\partial y} + \frac{\partial \boldsymbol{H}}{\partial z} = \boldsymbol{S}, \tag{29}$$

where $\boldsymbol{U}$, $\boldsymbol{F}$, $\boldsymbol{G}$ and $\boldsymbol{H}$ are given by (1–4) and the source terms are those in equations (25–27)

$$\boldsymbol{S} = [0, -\boldsymbol{B}\nabla\cdot\boldsymbol{B}, -(\boldsymbol{v}\cdot\boldsymbol{B})\nabla\cdot\boldsymbol{B}, -\boldsymbol{v}\nabla\cdot\boldsymbol{B}]^{\rm t}.$$

We start by defining a regular grid such that the i,j,k cell occupies the region $(i-1/2)h \le x \le (i+1/2)h$, $(j-1/2)h \le y \le (j+1/2)h (k-1/2)h \le z \le (k+1/2)h$, where h is the mesh spacing. Now suppose that we know the solution at $t = t_n$ and we want to calculate it at a later time t_{n+1}. We integrate equations (29) over the i,j,k cell and from $t = t_n$ to $t = t_{n+1}$ to get

$$\begin{aligned}&\frac{\boldsymbol{U}_{ijkn+1} - \boldsymbol{U}_{ijkn}}{t_{n+1} - t_n}\\ &+\frac{1}{h}(\boldsymbol{F}_{i+\frac{1}{2}jkn+\frac{1}{2}} - \boldsymbol{F}_{i-\frac{1}{2}jkn+\frac{1}{2}})\\ &+\frac{1}{h}(\boldsymbol{G}_{ij+\frac{1}{2}kn+\frac{1}{2}} - \boldsymbol{G}_{ij-\frac{1}{2}kn+\frac{1}{2}})\\ &+\frac{1}{h}(\boldsymbol{H}_{ijk+\frac{1}{2}n+\frac{1}{2}} - \boldsymbol{H}_{ijk-\frac{1}{2}n+\frac{1}{2}})\\ &= \boldsymbol{S}_{ijkn+\frac{1}{2}}.\end{aligned} \tag{30}$$

Here

$$\boldsymbol{U}_{ijkn} = \frac{1}{h^3}\int_V \boldsymbol{U}(\boldsymbol{r}, t_n)\mathrm{d}V$$

is the mean value of $\boldsymbol{U}$ in the ijk cell at time t_n and

$$\boldsymbol{F}_{i+\frac{1}{2}jkn+\frac{1}{2}} = \frac{1}{h^2(t_{n+1}-t_n)}\int_{t_n}^{t_{n+1}}\int_{S_{i+\frac{1}{2}}} \boldsymbol{F}\left[\left(i+\frac{1}{2}\right)h, y, z, t\right]\mathrm{d}S\mathrm{d}t,$$

$$\boldsymbol{G}_{ij+\frac{1}{2}kn+\frac{1}{2}} = \frac{1}{h^2(t_{n+1}-t_n)}\int_{t_n}^{t_{n+1}}\int_{S_{j+\frac{1}{2}}} \boldsymbol{G}\left[x, \left(j+\frac{1}{2}\right)h, z, t\right]\mathrm{d}S\mathrm{d}t,$$

$$\boldsymbol{H}_{ijk+\frac{1}{2}n+\frac{1}{2}} = \frac{1}{h^2(t_{n+1}-t_n)}\int_{t_n}^{t_{n+1}}\int_{S_{k+\frac{1}{2}}} \boldsymbol{H}\left[x, y, \left(k+\frac{1}{2}\right)h, t\right]\mathrm{d}S\mathrm{d}t,$$

are the fluxes averaged over time and the cell interfaces, $S_{i+\frac{1}{2}}$, $S_{j+\frac{1}{2}}$ and $S_{k+\frac{1}{2}}$.

$$\boldsymbol{S}_{ijkn+\frac{1}{2}} = \frac{1}{h^3(t_{n+1}-t_n)}\int_{V_{ijk}} \boldsymbol{S}(\boldsymbol{r}, t)\mathrm{d}V$$

is the source term averaged over time and the cell volume, V_{ijk}.

4.1 First-order scheme

Equation (30) is exact and forms the basis of all conservative schemes. In a first-order Godunov-type scheme (Godunov 1959), the approximations to the fluxes and source terms are determined by assuming that the solution is uniform within each cell and constant over a time step. Thus, if $\boldsymbol{U}_*(\boldsymbol{U}_{\rm L}, \boldsymbol{U}_{\rm R})$ is the state at the position of the initial discontinuity, the first-order fluxes are

$$\boldsymbol{F}_{i+\frac{1}{2}jkn+\frac{1}{2}} = \boldsymbol{F}[\boldsymbol{U}_*(\boldsymbol{U}_{ijkn}, \boldsymbol{U}_{i+1jkn})],$$

$$\boldsymbol{G}_{ij+\frac{1}{2}kn+\frac{1}{2}} = \boldsymbol{G}[\boldsymbol{U}_*(\boldsymbol{U}_{ijkn}, \boldsymbol{U}_{ij+1kn})],$$

$$\boldsymbol{H}_{ijk+\frac{1}{2}n+\frac{1}{2}} = \boldsymbol{H}[\boldsymbol{U}_*(\boldsymbol{U}_{ijkn}, \boldsymbol{U}_{ijk+1n})].$$

In curvilinear coordinates one has to be careful how the source term is approximated (Falle 1991), but in cartesian coordinates there is no difficulty. If the source term depended only on $\boldsymbol{U}$, the first-order approximation would be

$$\boldsymbol{S}_{ijkn+\frac{1}{2}} = \boldsymbol{S}(\boldsymbol{U}_{ijkn}).$$

In this case the source term depends on $\nabla\cdot\boldsymbol{B}$ as well as $\boldsymbol{U}$ and we therefore need an approximation to $\nabla\cdot\boldsymbol{B}$. Since these terms arise because the equations are not conservative when $\nabla\cdot\boldsymbol{B} \neq 0$, we should determine $\nabla\cdot\boldsymbol{B}$ from the fields used to compute the fluxes i.e.

$$\begin{aligned}(\nabla\cdot\boldsymbol{B})_{ijkn} = \frac{1}{h}[&(B_x)_{i+\frac{1}{2}jkn} - (B_x)_{i-\frac{1}{2}jkn}\\ &+(B_y)_{ij+\frac{1}{2}kn} - (B_y)_{ij-\frac{1}{2}kn}\\ &+(B_z)_{ijk+\frac{1}{2}n} - (B_z)_{ijk+\frac{1}{2}n}].\end{aligned}$$

Since the field perpendicular to the cell interfaces is the average of that in the adjoining cells, this amounts to using central differences.

4.2 Second-order scheme

In order to achieve second-order accuracy, we use the first-order scheme to obtain the solution, $\boldsymbol{U}_{n+\frac{1}{2}}$ at the half time, $t_{n+\frac{1}{2}}$ and then use this to compute average gradients in each cell as follows

$$\left(\frac{\partial\boldsymbol{P}}{\partial x}\right)_{ijkn+\frac{1}{2}} = \frac{1}{h}\,\mathrm{av}(\boldsymbol{P}_{ijkn+\frac{1}{2}} - \boldsymbol{P}_{i-1jkn+\frac{1}{2}}, \boldsymbol{P}_{i+1jkn+\frac{1}{2}} - \boldsymbol{P}_{ijkn+\frac{1}{2}}),$$

$$\left(\frac{\partial\boldsymbol{P}}{\partial y}\right)_{ijkn+\frac{1}{2}} = \frac{1}{h}\,\mathrm{av}(\boldsymbol{P}_{ijkn+\frac{1}{2}} - \boldsymbol{P}_{ij-1kn+\frac{1}{2}}, \boldsymbol{P}_{ij+1kn+\frac{1}{2}} - \boldsymbol{P}_{ijkn+\frac{1}{2}}),$$

$$\left(\frac{\partial\boldsymbol{P}}{\partial z}\right)_{ijkn+\frac{1}{2}} = \frac{1}{h}\,\mathrm{av}(\boldsymbol{P}_{ijkn+\frac{1}{2}} - \boldsymbol{P}_{ijk-1n+\frac{1}{2}}, \boldsymbol{P}_{ijk+1n+\frac{1}{2}} - \boldsymbol{P}_{ijkn+\frac{1}{2}}),$$

where $\mathrm{av}(a,b)$ is a non-linear averaging function, the purpose of which is to reduce the scheme to first order in the neighbourhood of discontinuities. This is necessary since Godunov's theorem (Godunov 1959) tells us that a scheme that is second order everywhere will not be monotonic near discontinuities. The averaging function must be homogeneous of degree one and have the properties

$$\begin{aligned}\mathrm{av}(a,b) &= \tfrac{1}{2}(a+b) \ \text{ as } a \to b,\\ &= 0 \qquad\quad \text{if } ab < 0,\\ &\to a \qquad\quad \text{as } |a|/|b| \to 0,\\ &\to b \qquad\quad \text{as } |b|/|a| \to 0.\end{aligned}$$

There are obviously an infinite number of functions with these properties and there is no general agreement about which is best. We will adopt the following simple prescription,

$$\begin{aligned}\mathrm{av}(a,b) &= \frac{(a^2b + ab^2)}{(a^2+b^2)} \ \text{ if } a^2 + b^2 \neq 0 \text{ and } ab > 0,\\ &= 0 \qquad\qquad \text{otherwise,}\end{aligned}$$

which obviously has the correct properties (van Leer 1977).

These gradients can now be used to set up the left and right states for the second-order Riemann problems. For the fluxes in the x direction we have

$$\boldsymbol{P}_{\mathrm{L}} = \boldsymbol{P}_{ijkn+\frac{1}{2}} + \frac{1}{2}h\left(\frac{\partial\boldsymbol{P}}{\partial x}\right)_{ijkn+\frac{1}{2}}$$

$$\boldsymbol{P}_{\mathrm{R}} = \boldsymbol{P}_{i+1jkn+\frac{1}{2}} - \frac{1}{2}h\left(\frac{\partial\boldsymbol{P}}{\partial x}\right)_{i+1jkn+\frac{1}{2}}$$

$$\boldsymbol{F}_{i+\frac{1}{2}jkn+\frac{1}{2}} = \boldsymbol{F}[\boldsymbol{U}_*(\boldsymbol{P}_{\mathrm{L}}, \boldsymbol{P}_{\mathrm{R}})],$$

and similarly for those in the y and z directions.

The second-order source term is computed from $\boldsymbol{U}_{n+\frac{1}{2}}$ in the same way as for the first-order scheme. This means that $\nabla\cdot\boldsymbol{B}$ is still obtained from a central difference in smooth regions, but the averaging function turns it into a one-sided difference at discontinuities.

Although this scheme requires that the Riemann problem be solved twice at each interface, it is genuinely second order and the fact that it is not operator split makes it easy to ensure that source terms are approximated to second order. Roe-type schemes are not strictly second order since they do not take into account the change in the mean matrix over a time step. This scheme has proved to be accurate and robust, both for ordinary gas dynamics (Falle 1991) and relativistic hydrodynamics (Falle & Komissarov 1996).

4.3 Artificial dissipation

Although upwind schemes of this type generally perform very well, they are inclined to misbehave in regions where the dissipation generated by the truncation errors becomes small or very anisotropic. This can lead to unphysical distortions of shock fronts and a non-linear instability for plane shocks that are nearly aligned with the grid (Quirk 1994). Adding some extra dissipation to the Riemann solver removes these problems and also reduces the long-wavelength entropy errors that occur behind slowly moving shocks (Roberts 1988).

Since the extra dissipation is only needed at shocks, we have to be careful that we do not degrade the accuracy of the scheme in smooth regions. We therefore use the left and right states in the Riemann problem to determine a diagonal viscous stress tensor, $\mathbf{S}$,

Table 1. Parameters for the test cases. BW – Brio & Wu; AW – Alfvén wave; FS – fast shock; SS – slow shock; FR – fast rarefaction; SR – slow rarefaction; OFS – oblique fast shock (note that these are the states for a shock whose normal is parallel to the x-axis).

Case	Left State	Right State
BW	$\rho = 1, p_{\mathrm{g}} = 1, \boldsymbol{v} = (0,0,0), \boldsymbol{B} = (0.75, 1, 0)$	$\rho = 0.125, p_{\mathrm{g}} = 0.1, \boldsymbol{v} = (0,0,0), \boldsymbol{B} = (0.75, -1, 0)$
AW	$\rho = 1, p_{\mathrm{g}} = 1, \boldsymbol{v} = (0,1,1), \boldsymbol{B} = (1,1,0)$	$\rho = 1, p_{\mathrm{g}} = 1, \boldsymbol{v} = (0,1,1), \boldsymbol{B} = (1,1,0)$
FS	$\rho = 3, p_{\mathrm{g}} = 16.33, \boldsymbol{v} = (-0.732, -1.333, 0), \boldsymbol{B} = (3, 2.309, 1)$	$\rho = 1, p_{\mathrm{g}} = 1, \boldsymbol{v} = (-4.196, 0, 0), \boldsymbol{B} = (3,0,0)$
SS	$\rho = 1.368, p_{\mathrm{g}} = 1.769, \boldsymbol{v} = (0.269, 1.0, 0), \boldsymbol{B} = (1,0,0)$	$\rho = 1, p_{\mathrm{g}} = 1, \boldsymbol{v} = (0,0,0), \boldsymbol{B} = (1,1,0)$
FR	$\rho = 1, p_{\mathrm{g}} = 2, \boldsymbol{v} = (0,0,0), \boldsymbol{B} = (1,3,0)$	$\rho = 0.2641, p_{\mathrm{g}} = 0.2175, \boldsymbol{v} = (3.6, -2.551, 0), \boldsymbol{B} = (1,0,0)$
SR	$\rho = 1, p_{\mathrm{g}} = 2, \boldsymbol{v} = (0,0,0), \boldsymbol{B} = (1,0,0)$	$\rho = 0.2, p_{\mathrm{g}} = 0.1368, \boldsymbol{v} = (1.186, 2, 967, 0), \boldsymbol{B} = (1, 1.6405, 0)$
OFS	$\rho = 1, p_{\mathrm{g}} = 1, \boldsymbol{v} = (6.505, 1, 0), \boldsymbol{B} = (1,1,1)$	$\rho = 3, p_{\mathrm{g}} = 20.268, \boldsymbol{v} = (2.169, 1.331, 0.331), \boldsymbol{B} = (1, 3.153, 3.153)$

given by

$$\mathbf{S}_{xx} = \eta\rho^* c_{\rm f}^*(v_{x\rm R} - v_{x\rm L}),$$
$$\mathbf{S}_{yy} = \eta\rho^* c_{\rm f}^*(v_{y\rm R} - v_{y\rm L}), \qquad (31)$$
$$\mathbf{S}_{zz} = \eta\rho^* c_{\rm f}^*(v_{z\rm R} - v_{z\rm L}),$$

where $\rho^*, c_{\rm f}^*$ are the density and fast speed in the resolved state and η is a dimensionless parameter. In all our calculations we have set $\eta = 0.15$.

In those places where the scheme reduces to first order we have $|\boldsymbol{v}_{\rm L} - \boldsymbol{v}_{\rm R}| \propto h$ and (31) therefore corresponds to a kinematic viscosity, ν, of the form

$$\nu = \eta c_{\rm f} h,$$

whereas in smooth regions $|\boldsymbol{v}_{\rm L} - \boldsymbol{v}_{\rm R}| \propto h^2$ and the viscous fluxes are of second order. The order of the scheme in such places is therefore not reduced by the addition of these fluxes.

5 TESTS

Since codes of this type are designed for flows containing shocks, it is customary to test them on various Riemann problems. We start with the shock tube problem considered by Brio & Wu (1988), which is a MHD version of the Sod problem (Sod 1978). The parameters for this, together with those for our other test problems, are given in Table 1.

Fig. 1 shows the results both for a strictly one-dimensional calculation and a two-dimensional one in which the initial discontinuity makes an angle of 45° with grid. In both cases the quality of our solution is the same as that obtained by Brio & Wu with the same numerical resolution. The transverse field changes sign in this case, so this shows that our simple method of dealing with degeneracy works just as well as their more complicated one. The results for the two-dimensional calculation are almost as good except that there is small jump in the normal field at the discontinuities. This hardly surprising given that the initial state actually consist of a series of steps and therefore does not satisfy $\nabla\cdot\boldsymbol{B} = 0$. Apart from that, the shock conditions are pretty accurately satisfied even though the code is not strictly conservative. This is gratifying because, although Fig. 1 shows that $\nabla\cdot\boldsymbol{B}$ is only appreciably different from zero in the the discontinuities, the fact that the calculation fails if we do not include the extra terms in the equations tells us that they are playing a significant role. It has to be said that this case is not a very stringent test of this since the shocks are quite weak, but we shall see later that the results are similar for a strong fast shock.

As Brio & Wu have already pointed out, the numerical solution contains an intermediate shock and a compound wave. It is well known (see e.g. Jeffrey & Taniuti 1964) that intermediate shocks are non-physical and that the solution to the Riemann problem may not be unique if such shocks are allowed. This particular problem is an example of this and Fig. 2 shows an alternative solution in which the sign of the transverse field is reversed by an Alfvén wave instead of an intermediate shock. The fact that all numerical schemes seem to generate an intermediate shock in this case is simply because the velocity and the magnetic field define the same plane everywhere. Such coplanar problems are clearly rather special and, like Barmin, Kulikovskiy & Pogorelov (1996), we find that our numerical scheme does not generate intermediate shocks for more generic data. The existence of intermediate shocks is, however, a subtle question and we prefer to postpone discussion of this to a later paper. It is nevertheless worth pointing out that we get the same numerical solution for this initial data if we use an exact Riemann solver.

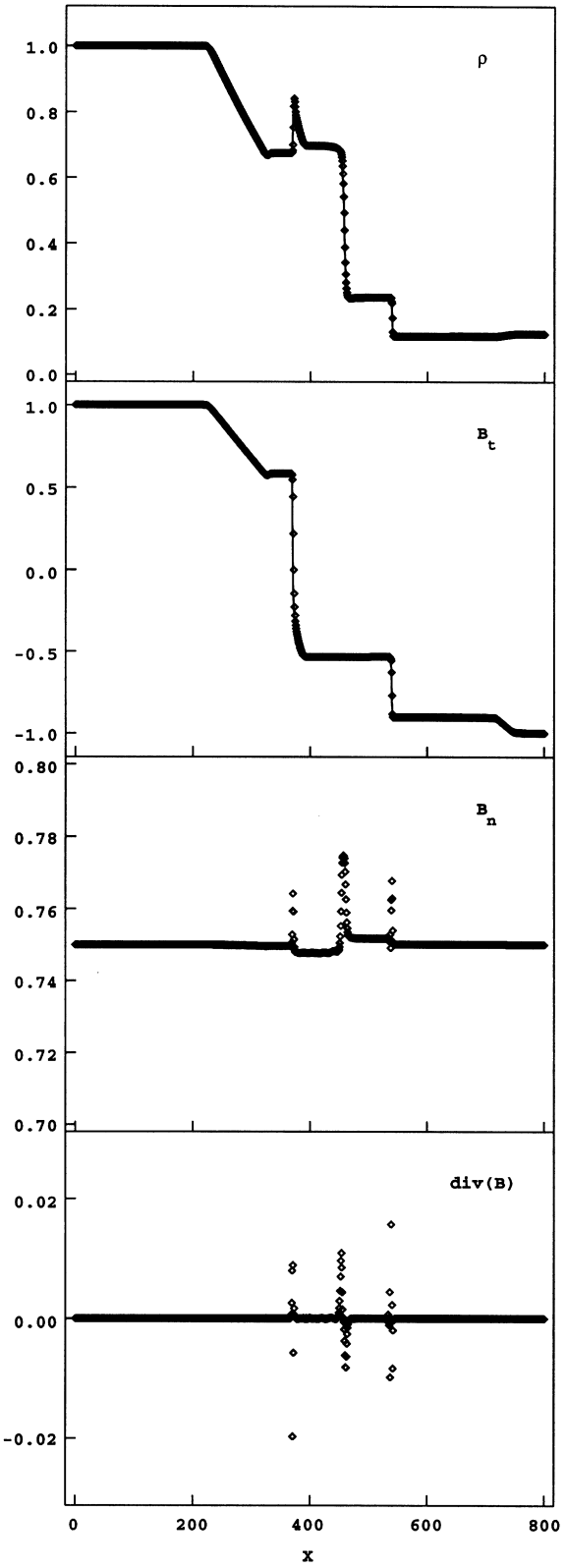

Figure 1. Density, transverse field, normal field and $\nabla\cdot\boldsymbol{B}$ for the Brio & Wu problem (BW). The line is a one-dimensional calculation and the points are a two-dimensional one in which the initial discontinuity makes an angle of 45° with the axes.

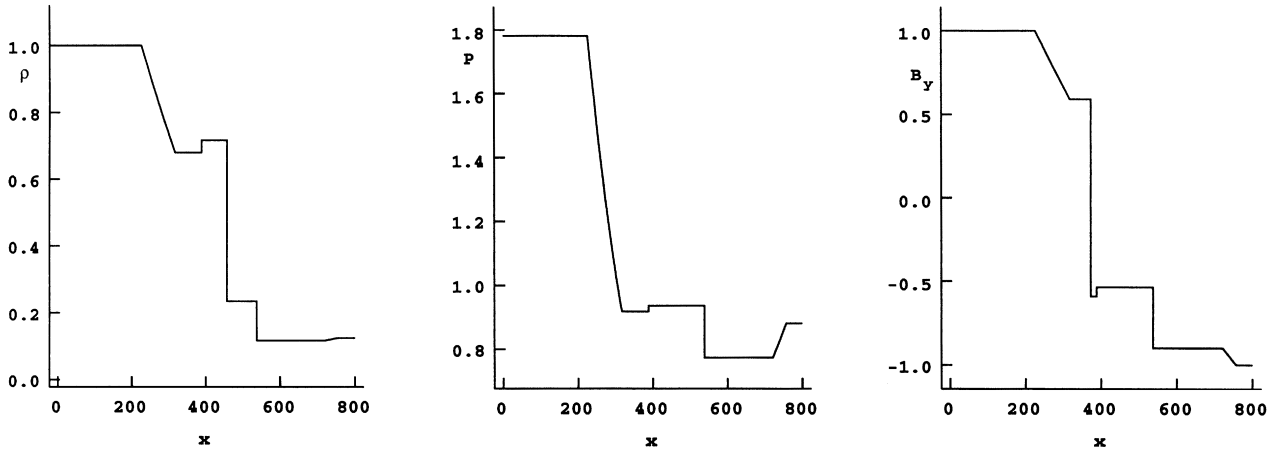

Figure 2. Density, total pressure and transverse field for a solution to the Brio & Wu problem (BW) that does not contain an intermediate shock. This was obtained with the exact Riemann solver described in Section 2.2.

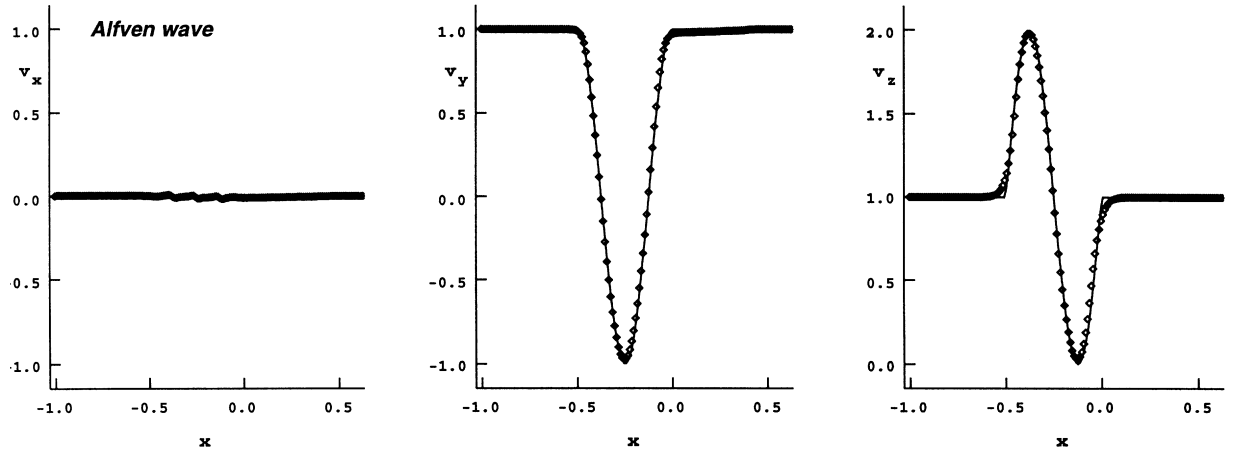

Figure 3. x, y, and z velocity in an Alfvén wave which rotates the field through 2π (AW). The wave has travelled a distance of three times its width. The points are the numerical solution and the line is the exact solution.

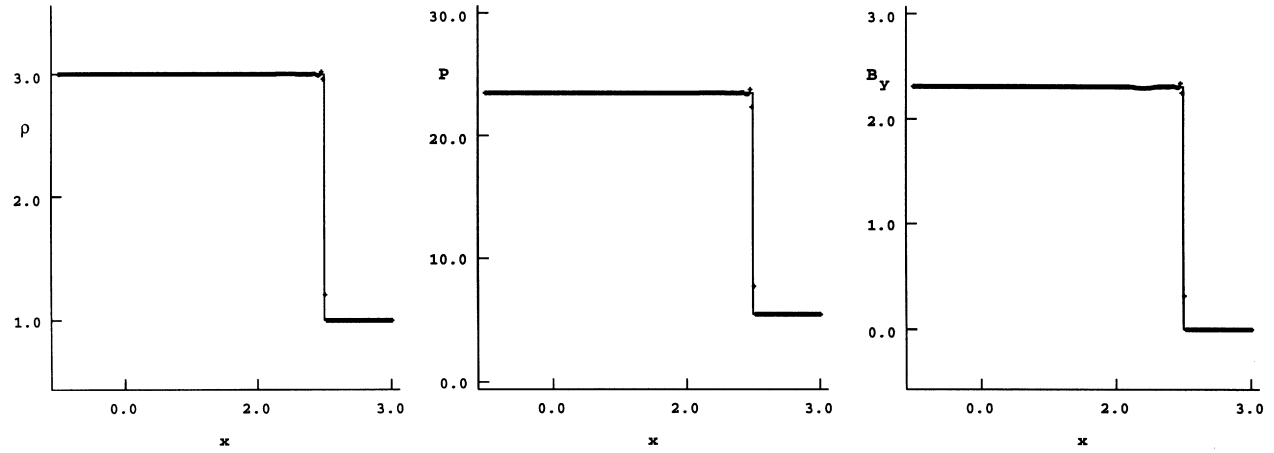

Figure 4. Density, total pressure and transverse field in a fast switch-on shock (FS). The points are the numerical solution and the line is the exact solution.

The fact that the solution to the Brio & Wu problem contains a number of different waves makes it a good test of a numerical scheme, but it is somewhat controversial. Although there are many other types of MHD Riemann problems, we believe that the most rational procedure is to test our code with a complete set of pure waves i.e. shocks, contact discontinuities, Alfvén waves and centred rarefactions.

Fig. 3 shows the results for a single wavelength of a sinusoidal Alfvén wave in which the tangential component of the field rotates through 2π. It can be seen that the errors are undetectable except for

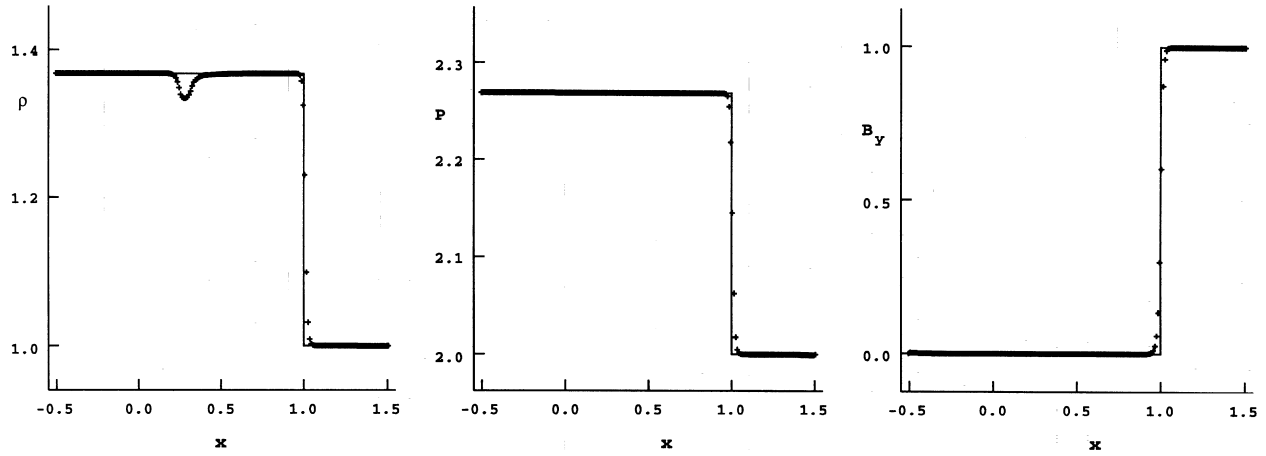

Figure 5. Density, total pressure and transverse field in a slow switch-off shock (SS). The points are the numerical solution and the line is the exact solution.

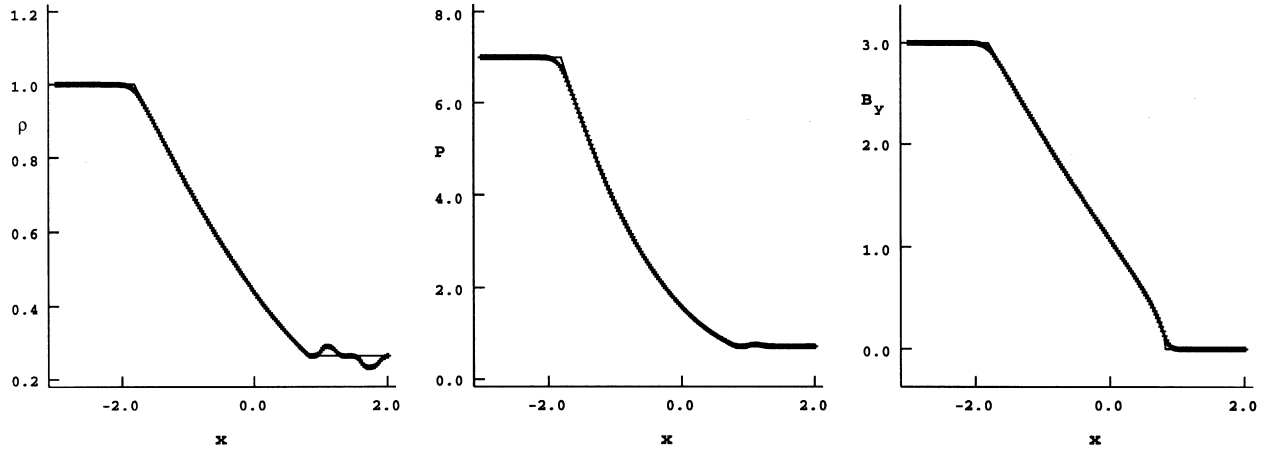

Figure 6. Density, total pressure and transverse field in a fast switch-off rarefaction (FR). The points are the numerical solution and the line is the exact solution.

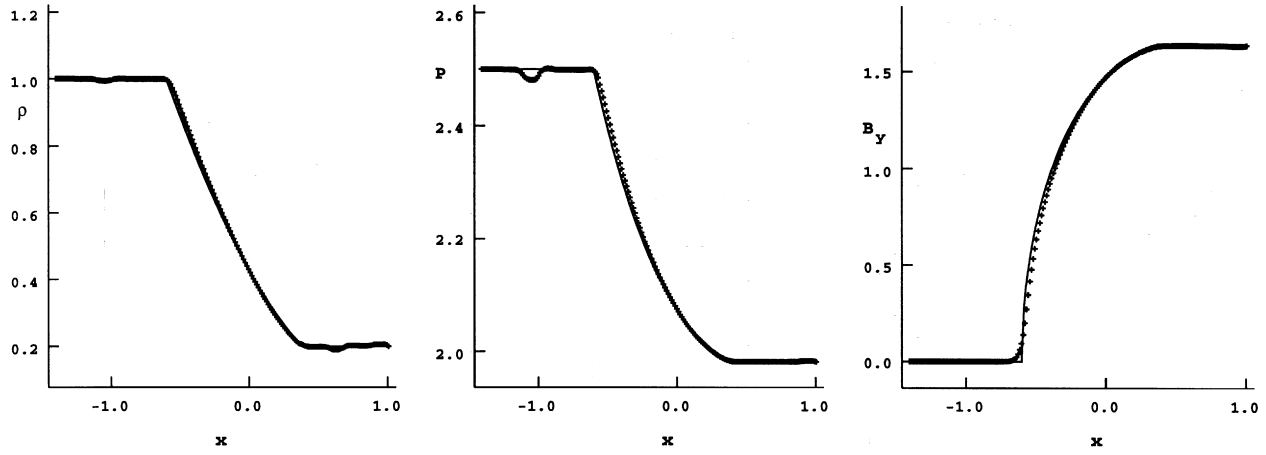

Figure 7. Density, total pressure and transverse field in a slow switch-on rarefaction (SR). The points are the numerical solution and the line is the exact solution.

some numerical diffusion at the discontinuity in the gradient at the leading and trailing edge of the wave. Such errors are, of course, unavoidable in schemes of this type. Note that, although Alfvén waves are linearly degenerate in the sense that the wavespeed is constant in the wave, the eigenvectors are not unless we write them in terms of the magnitude and angle of the transverse field. The linearized Riemann solver is therefore not exact. However, in this case the wave is so well-resolved that it does not make any difference which Riemann solver we use.

As a further test of our procedure for handling degeneracy, we chose our fast and slow shocks to be switch on and switch off shocks respectively. We can see froms Figs 4 and 5 that the code handles both of these extremely well with about four mesh points in the slow shock and three in the fast shock. Although this is wider than many

people would like, the width of the shock structure does not just depend upon the scheme, but also on the strength of the shock and its speed relative to the grid. If we had chosen the left and right states so that the shocks are stationary on the grid and there were no artificial viscosity, then the jumps would have been only one mesh point wide. This is because our linearized Riemann solver always chooses the upstream state when confronted with a stationary shock. Since the flux in this state is the same as that in the downstream state, the result is that the initial solution remains unchanged. Although it could pick either the upstream or downstream state, an exact Riemann solver produces exactly the same result because both these states have the same fluxes.

While such sharp shocks look impressive, they are highly undesirable in multidimensional calculations. To see this, consider a steady flow with a curved shock. Any part of the shock that is closely aligned with the grid will be much thinner than those parts that are not, which tends to produce large errors at the point where the shock thickness changes. As we have already pointed out in Section 4.3, this can be avoided by introducing extra dissipation in regions in which the second derivatives are large. Since this only affects very thin shock structures, it makes no discernible difference to the numerical results in Figs 3 and 4.

Apart from the finite width of the shock, the only other errors in Figs 4 and 5 are some small-amplitude waves, which travel away from the shock. These are generated as the initially discontinuity evolves into a steadily propagating shock with finite width. All shock capturing schemes do this when they are given discontinuous initial data.

Start-up waves are also generated in the fast and slow rarefaction waves (Figs 6 and 7) because of the $O(1)$ errors that inevitably arise when the initial discontinuity spreads out. They would not have appeared had we started the rarefactions with finite width.

In order to test the various Riemann solvers to destruction, we have deliberately chosen quite strong switch-on and switch-off rarefactions. We find that both linearized Riemann solvers fail for these cases unless we include explicit artificial dissipation. This is in contrast to both ordinary and relativistic gas dynamics, where Riemann solver B can handle anything except two strong rarefactions. The reason for this is that in ordinary or relativistic gas dynamics, Riemann solver B can only generate a resolved state with a negative pressure if there are two strong rarefactions, whereas in MHD it can do so even if there is only a single rarefaction. There is, of course, no such problem with the exact Riemann solver.

Although all the results presented here were obtained with Riemann solver A, they are indistinguishable from those with Riemann solver B. This tells us that there is no point in using Riemann solver B since it is no better than A and is much more expensive. Strong rarefactions can be handled either by using artificial dissipation and a finite floor pressure in the resolved state, or by using the exact solver if the Riemann solution contains strong rarefactions. The former is easier, but the latter is more intellectually respectable.

Our final test is designed see how much damage the monopole source terms do to the jump conditions at strong shocks. Since the shocks in the two-dimensional Brio & Wu problem are not really strong enough to do this, we computed a strong fast shock (case OBF) at an angle of 45° to the x-axis. We can see from Fig. 8 that, apart from the usual start-up waves, the only significant error is that the normal component of the field changes across the shock by about the same fraction as it does in the Brio & Wu problem. Although this is larger than one would like, it is encouraging that it is no worse for strong shocks than it is for weak ones. This suggests

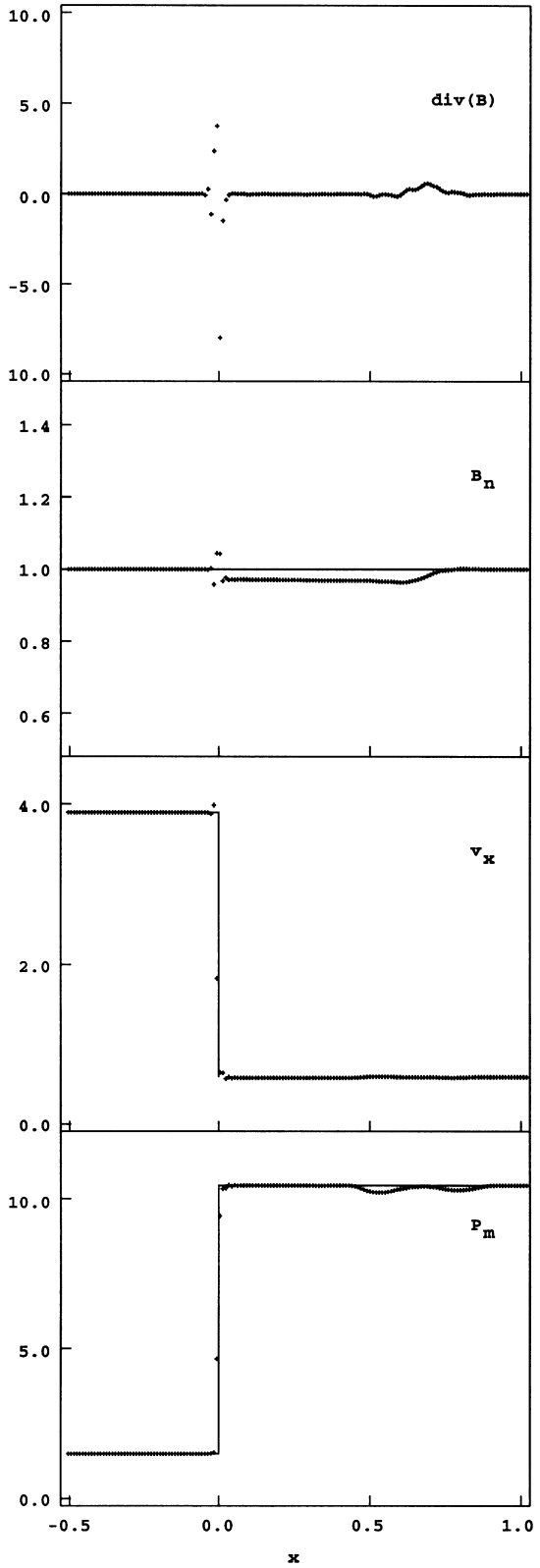

Figure 8. $\nabla\cdot\boldsymbol{B}$, normal magnetic field, x velocity and magnetic pressure in a two dimensional calculation of a strong fast shock which make an angle of 45° with the axes (OBF). The points are the numerical solution and the line is the exact solution.

that the error occurs because the initial states in these numerical calculations do not satisfy $\nabla\cdot\boldsymbol{B} = 0$ and has nothing to do with our failure to satisfy strict conservation at shocks.

Although the scheme fails on two-dimensional problems with an initial discontinuity in the field if monopole source terms are not included, it can manage without them if the initial discontinuity is smeared over a few mesh points. This is consistent with the fact that Zachary, et al. (1994) found that it made no difference whether or not they used a pseudo-potential to correct the field in their two-dimensional calculations with an initially continuous field. It would, however, be unwise to conclude from this that these terms can be ignored. Even if one confines oneself to initially continuous fields, the numerical monopoles can still cause problems in places where the physical forces are close to equilibrium.

This case also provides a further demonstration of the value of adding extra dissipation at shocks. The shock is stationary on the grid and would therefore be very sharp if we relied on the dissipation owing to the truncation errors. In fact, it is so sharp that the scheme fails if we do not include extra dissipation.

Finally, it is worth mentioning that neither Riemann solver A nor B have any trouble with the one-dimensional Riemann problems considered by Zachary et al. (1994) or Ryu & Jones (1995).

6 CONCLUSIONS

Although our scheme is very similar to the ones devised other by authors, it has a number of features which make it more reliable and robust. Even if one is only interested in one dimensional problems, both Brio & Wu and Ryu & Jones recommend Riemann solver A, which, as we have shown, fails on strong, initially discontinuous rarefaction waves. Fortunately, we find that this can be cured either by adding artificial viscosity, or by using an exact solver whenever the solution to the Riemann problem contains strong rarefactions. We have also shown that there is a much simpler way of dealing with the case of zero transverse field than the one proposed by Brio & Wu (1988).

A purely one-dimensional scheme is not particularly useful, so it is gratifying that ours also works in multidimensions. As is well known, the condition $\nabla\cdot\boldsymbol{B} = 0$ means that it is not a trivial matter to extend a one-dimensional scheme to multidimensions. Of the various ways of dealing with this, adding terms to undo the effect of the numerical monopoles is by far the simplest. Although it might seem dangerous to allow numerical monopoles to exist, both our results and those of Powell (1994) suggest that they do not cause any trouble. They are only significant in the neighbourhood of discontinuities and the fact that almost equal amounts of positive and negative monopoles are generated in close proximity to each other means that they are unlikely to do too much damage to the field topology.

Finally, it is somewhat bizarre that the Brio & Wu problem, which contains intermediate shocks and compound waves, has become a standard test problem for upwind MHD codes. As Dai & Woodward (1994) have suspected and we have shown there is an alternative solution to this problem, which does not contain such structures. Despite this, all sound numerical schemes should reproduce the solution containing intermediate shocks. This is clearly something which requires further work, but it is such a complex and subtle question that we prefer to postpone it to a later paper.

ACKNOWLEDGMENTS

We are grateful to the referee, G. Mellema, for a number of helpful suggestions. PJ acknowledges support from PPARC during the course of this work.

REFERENCES

Barmin A. A., Kulikovskiy A. G., Pogorelov N. V., 1996 J. Comp. Phys., 126, 77
Brackbill J. U., Barnes D. C., 1980 J. Comp. Phys., 35, 426
Brio M., Wu C. C., 1988 J. Comp. Phys., 75, 400
Cabannes H., 1970, Theoretical Magnetofluiddynamics. Academic Press, New York
Dai W., Woodward P. R., 1994 J. Comp. Phys., 111, 354
Eulderink F., Mellema G., 1994, A&A, 284, 654
Falle S. A. E. G., 1991, MNRAS, 250, 581
Falle S. A. E. G., Komissarov S. S., 1996, MNRAS, 278, 586
Font J. A., Ibáñez J. M., Marquina A., Martí J. M., 1994, A&A, 282, 304
Godunov S. K., 1959, Mat. Sb., 47, 357
Gogosov V. V., 1961 J. Appl. Math. Mech., 25, 148
Jeffreys A, Taniuti T., 1964, Non-linear Wave Propagation. Academic Press, New York
Kulikovskiy A. G., Lyubimov G. A., 1965, Magnetohydrodynamics. Addison-Wesley, Reading, Massachusetts
Parker E. N. 1979, Cosmical Magnetic Fields. Clarendon Press, Oxford
Powell K. G., 1994, ICASE Report No. 94-24. Langley, VA
Quirk J. J., 1994, Int. J. Num. Methods in Fluids, 18, 555
Roberts T. W., 1988 in Morton K. W., Baines M. J., eds, Numerical Methods for Fluid Dynamics 3. Clarendon Press, Oxford p. 442
Roe P. L., 1981 J. Comp. Phys., 43, 357
Roe P. L., 1986, Ann. Rev. Fluid Mech., 18, 337
Ryu D., Jones T. W., 1995, ApJ, 442, 228
Sod G. A., 1978 J. Comp. Phys., 49, 1
van Leer B., 1977 J. Comp. Phys., 23, 276
Zachary A. L., Malagoli A., Collela P., 1994, Siam J. Sci. Compu., 15, 263

This paper has been typeset from a TEX/LATEX file prepared by the author.